Supplementary information

Anisotropic magnetoresistance as evidence of spin-momentum inter-locking in topological Kondo insulator SmB_6 nanowires

Yugui Cui, Yi Chu, Zhencun Pan, Yingjie Xing, Shaoyun Huang*, Hongqi Xu*

Beijing Key Laboratory of Quantum Devices, Key Laboratory for the Physics and Chemistry of Nanodevices, and Department of Electronics, Peking University, Beijing, 100871, P. R. China.

Note 1: Single-crystalline SmB_6 nanowires grown by CVD.

The SmB_6 nanowires are synthesized using Samarium chloride ($SmCl_3$) (purity 99.99%, ALADDIN, China), boron trioxide (B_2O_3) and boron (B) (weight ratio 1:1, purity 99.99%, CNM, China) by CVD method. $SmCl_3$ is for the source of samarium. The mixture of B and B_2O_3 is heated to generate gaseous B_2O_2. SmB_6 particles washed by hydrochloric acid are dispersed on a Si substrate to help the growth of nanowires. The source and the substrate are placed in a quartz tube which is heated in a tube furnace. The heating temperature of the tube furnace is 1100 ^{O}C and the heating duration is 1~2 hours. A mixture of Argon (285 SCCM) and hydrogen (30 SCCM) is used as a carrier gas.

Note 2: Element mapping by EDAX.

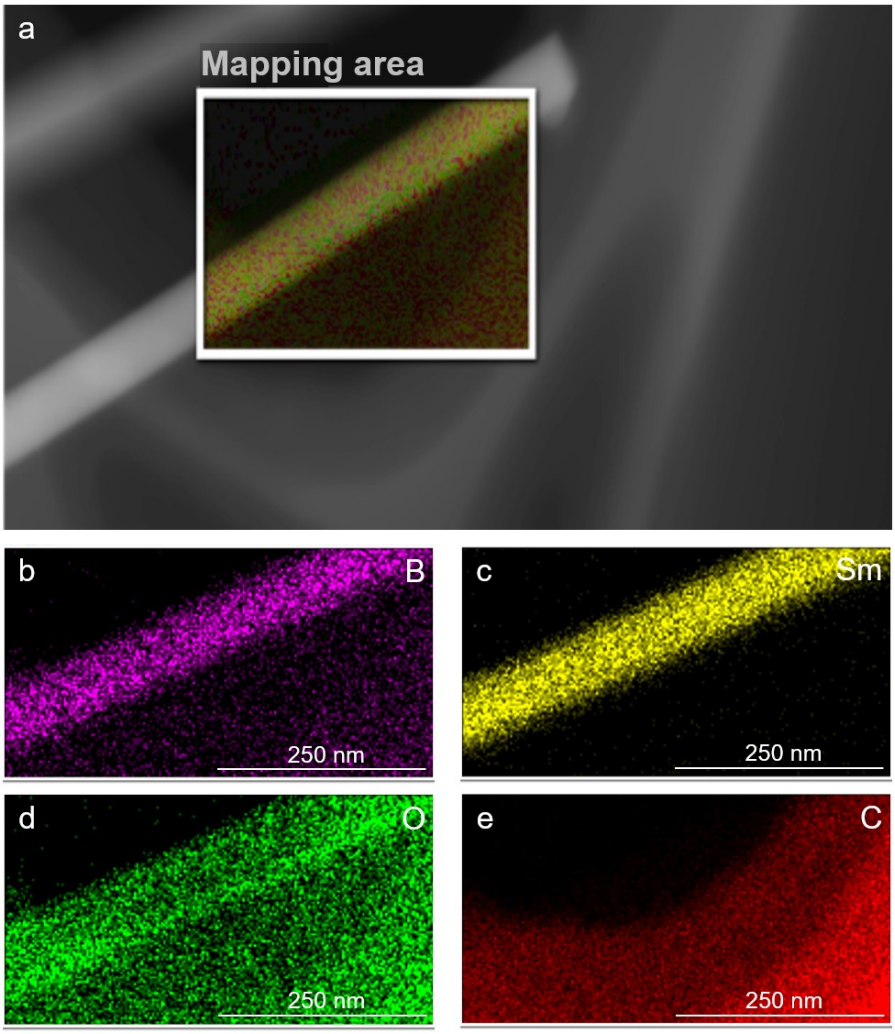

Figure S1. Representative EDAX mapping images of an individual SmB_6 nanowire. (a) SEM image. The inset indicates Sm and B distributions simultaneously; EDAX mapping of (b) B, (c) Sm, (d) O and (e) C.

Figure S1 shows the EDAX element mapping images of an individual SmB_6 nanowire. Figure S1(a) exhibits a selected SmB_6 nanowire as the mapping area, in which Sm and B distributions are displayed simultaneously. The individual mapping on elements of B, Sm, O, and C is displayed in Figure S1(b), (c), (d) and (e), respectively. The elements of B and Sm are found homogeneously distributed in the nanowire. The element of C comes from the carbon film covered copper grid and the element of O comes from the carbon film and/or the thin sheath of the nanowire.

Note 3: Characteristic temperatures.

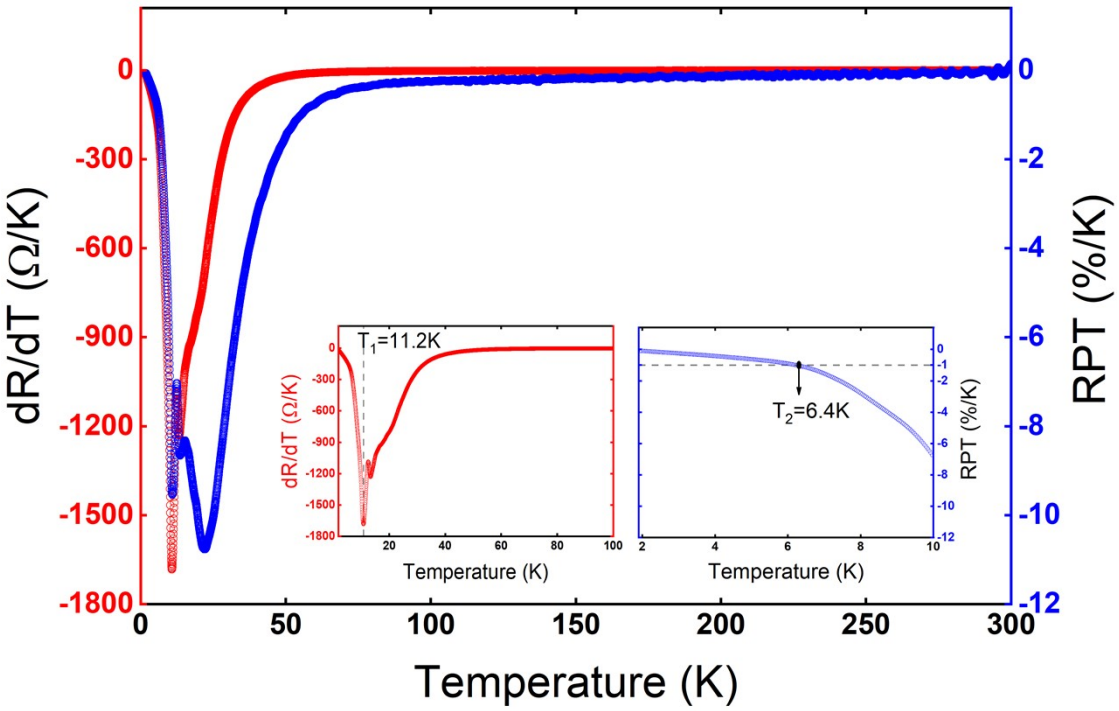

Figure S2. Characteristic temperatures of T_1 and T_2. The red dotted line shows the first-order differential temperature dependences of resistance. The blue dotted line shows the relative change of resistance per unit temperature (RPT). The inset of left panel shows a zoom-in of red line between 1.9 and 100 K. A characteristic temperature where the absolute change rate of resistance reaches its maximum is thus defined as T_1. The inset of right panel shows a zoom-in of blue line between 1.9 and 10 K. A characteristic temperature that indicates a resistance saturation with further lowing temperature is defined as T_2.

In this work, T_1 is defined as a characteristic temperature where the absolute change rate of resistance reaches its maximum. From the first-order differential temperature dependences of resistance, as shown in the inset on the left panel of Figure S2, T_1 = 11.2 K can be obtained. T_2 is defined as a characteristic temperature that indicates a resistance saturation with further lowing temperature. The relative change of resistance per unit temperature (RPT) can be written as followings

$$RPT = \frac{1}{R}\cdot\frac{dR}{dT}\cdot 100\%, \quad (1)$$

as shown by blue dotted-line in Figure S2. In case that the absolute RPT is lower than 1 %/K with further lowing temperature, the resistance is regarded to arrive at the saturation. We can obtain T_2 at 6.4 K, as shown in temperature dependences of RPT in the inset on the right panel of Figure S2.

The temperature dependences of resistance, as shown in Figure 2(a), can be separated into four characteristic regions by Kondo temperature (T_K), T_1 and T_2. Figure 2(b) shows the four regions from left to right at temperature from high to low one. In region *I*, a slight increase of resistance presents with decrease temperature from 300 K. The bulk states are dominant and the surface states can be ignored in the conductance because the Kondo screening effect is ignorable within this temperature range[1, 2]. In region *II* at temperature below T_K ~ 50 K, the *4f* flat band and *5d* conduction band of SmB_6 begin to hybridize with emergence of an energy gap[3]. As a consequence,

the resistance increases exponentially with decreasing temperature because the bulk states turn to vanish at Fermi level. Accordingly, the surface states start to contribute the conductance. In region *III*, where the temperature is below T_1 = 11.2 K, the contribution of surface states surpasses that of bulk states and the increase of resistance becomes slow with further decreasing temperature. In region *IV*, where the temperature decreasing below T_2 = 6.4 K, the surface states dominate the transport and the resistance arrives at a saturation.

Note 4: MR hysteresis.

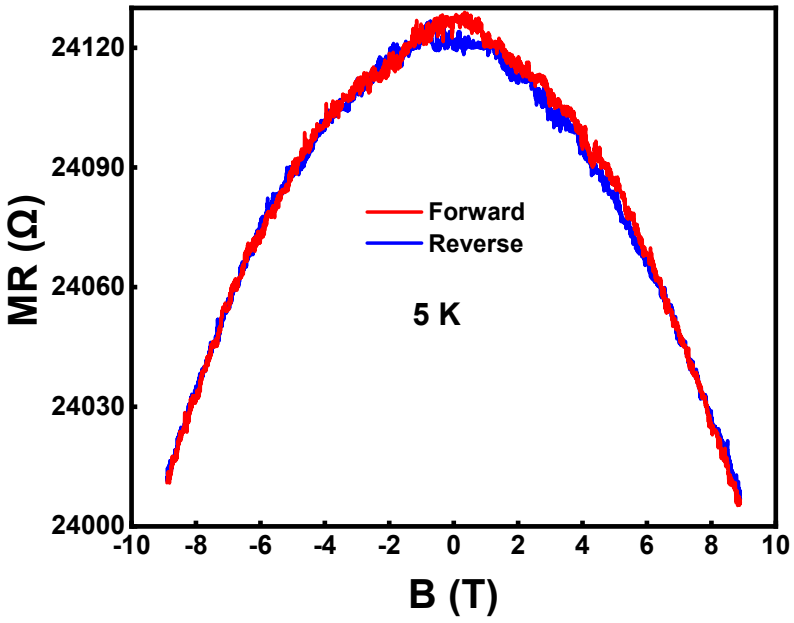

Figure S3. The MR in round-swept magnetic field. We measure the magnetic resistance at T = 5 K with θ = 45° by sweeping the magnetic field from -8.9 to 8.9 T (forward in red color), and reversing the magnetic field from 8.9 to -8.9 T (reverse in blue color).

Figure S3 shows the measured MR at T = 5 K with θ = 45° in round-swept magnetic field. Clearly, the MR is consistent each other in the forward and the reverse sweeps. There is no hysteresis in vicinity of zero magnetic field. The MR at B = -8.9 T in the forward and the reverse sweeps keeps unchanged within system errors. The localized *f* moments of bulk states are not in response to the external magnetic field and, therefore, completely quenched by cruising *d* electrons.

Note 5: Excitation current.

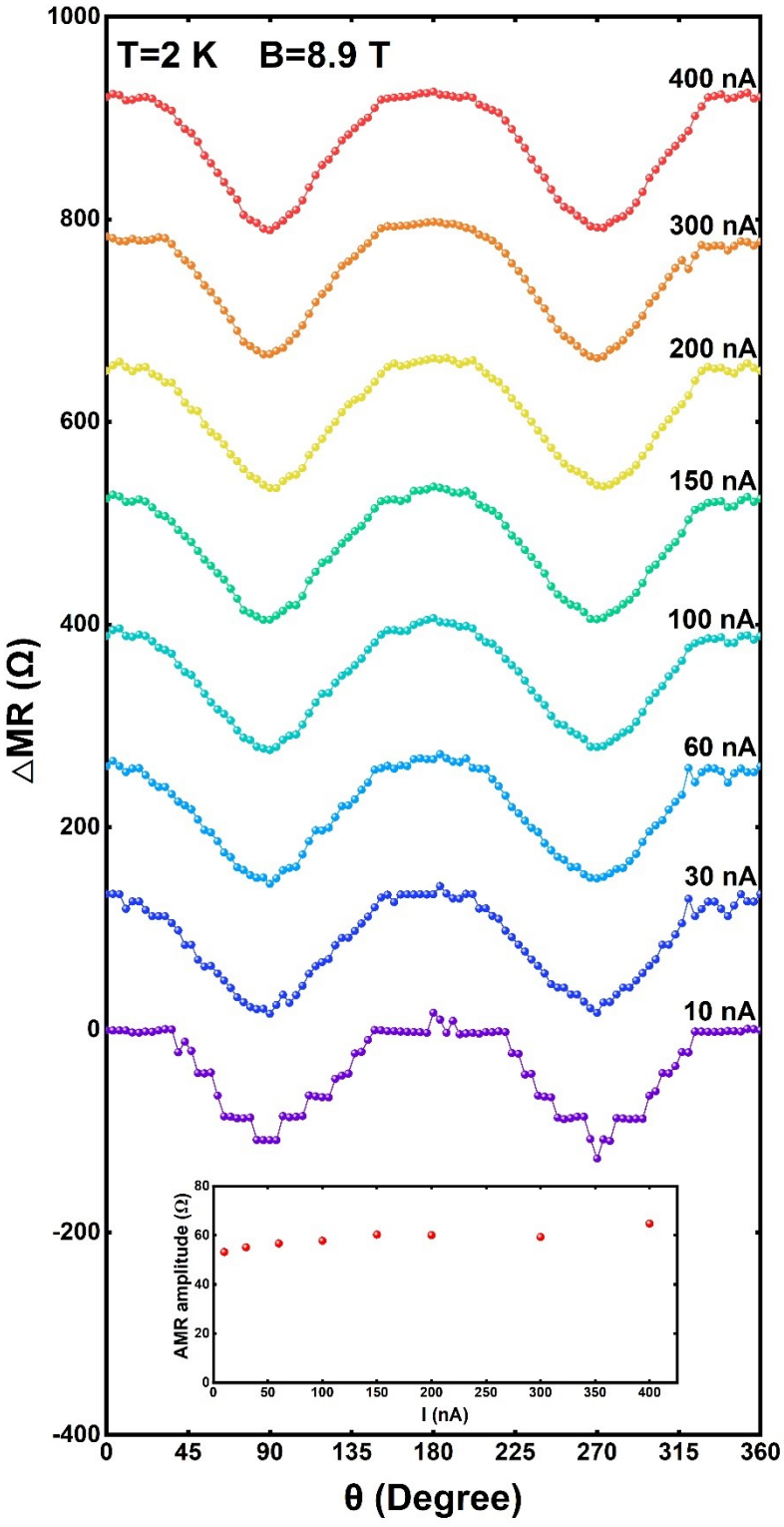

Figure S4. Excitation current dependences of anisotropic magnetoresistance. The AMR is measured using various excitation current at 1.8 K by a magnetic field strength of 8.9 T. For clarity, each data is offset accordingly.

Figure S4 shows the excitation current dependences of anisotropic magnetoresistance from 10 to 400 nA at 1.8 K by a constant magnetic field strength of 8.9 T from another device that

is similar with the device measured in this work. It can be seen that the signal-to-noise ratio of AMR improved by increasing the excitation current from 10 to 100 nA significantly. From 100 to 400 nA, the signal-to-noise ratio turns to saturate. For all measurement temperatures, however, the line-shape of AMR agrees well with the cosinoidal dependence of angle θ with a period of π and the AMR amplitude keeps constant within system errors, as shown in the inset. In this work, we choose the excitation current of 100 nA to perform MR measurements.

Note 6: Anisotropic magnetoresistance (AMR).

When an anisotropy of resistance is generated by an in-plane magnetic field, the resistance tensor could be presented by a diagonalization form in the principal coordinates of two-dimensional system. By taking the magnetic field direction as the *x'* axis of the principal coordinates, we have the relationship between electric field ($E_{x'}$, $E_{y'}$) and current density ($j_{x'}$, $j_{y'}$) as followings:

$$\begin{pmatrix} E_{x'} \\ E_{y'} \end{pmatrix} = \begin{pmatrix} MR_{//} & 0 \\ 0 & MR_{\perp} \end{pmatrix} \cdot \begin{pmatrix} j_{x'} \\ j_{y'} \end{pmatrix}$$

In the principal coordinates, $E_{x'}$ ($E_{y'}$) and $j_{x'}$ ($j_{y'}$) are along (perpendicular to) the magnetic field. This coordinate system should be transformed into the lab coordinate system, in which *x* is the measurement current direction and *y* is the transverse direction on the substrate plane. The transformation of the resistance tensor is in followings:

$$\begin{pmatrix} E_x \\ E_y \end{pmatrix} = \begin{pmatrix} cos\theta & -sin\theta \\ sin\theta & cos\theta \end{pmatrix} \cdot \begin{pmatrix} MR_{//} & 0 \\ 0 & MR_{\perp} \end{pmatrix} \cdot \begin{pmatrix} cos\theta & sin\theta \\ -sin\theta & cos\theta \end{pmatrix} \cdot \begin{pmatrix} j_x \\ j_y \end{pmatrix}$$

$$= \begin{pmatrix} MR_{//}cos^2\theta + MR_{\perp}sin^2\theta & (MR_{//} - MR_{\perp})cos\theta sin\theta \\ (MR_{//} - MR_{\perp})cos\theta sin\theta & MR_{//}sin^2\theta + MR_{\perp}cos^2\theta \end{pmatrix} \cdot \begin{pmatrix} j_x \\ j_y \end{pmatrix}$$

The measurement configuration of this work gives rise to the boundary condition of $j_y = 0$ and we can obtain the following conclusions:

$$MR_{xx} = E_x/j_x = MR_{//}cos^2\theta + MR_{\perp}sin^2\theta = MR_{\perp} + (MR_{//} - MR_{\perp})cos^2\theta = \frac{1}{2}(MR_{//} + MR_{\perp})$$

and

$$MR_{yx} = E_y/j_x = (MR_{//} - MR_{\perp})cos\theta sin\theta$$

Clearly, the presentation of MR_{xx} indicates that the equation (2) of main text holds. The normalization with regard to the amplitude of $(MR_{||} - MR_{\perp})/2$ highlight the origin of anisotropy, which is independent on temperature. On the other hand, the MR_{yx} represents the planar Hall effect (PHE), which is essentially an off-diagonal component of the in-plane magnetoresistance, is out of the topic of this work. The anisotropic magnetoresistance (AMR) manifests itself in MR_{xx} and is comprehensively addressed in this work to support the spin-moment locking of topological surface states.

References

[1] M. Dzero, J. Xia, V. Galitski,P. Coleman. *Annu. Rev. Condens. Matter Phys.* **2016**,7,249.

[2] A. Tytarenko, K. Nakatsukasa, Y. K. Huang, S. Johnston,E. v. Heumen. *New J. Phys.* **2016**,18,123003.

[3] S. Wolgast, Ç. Kurdak, K. Sun, J. W. Allen, D.-J. Kim,Z. Fisk. *Phys. Rev. B*

2013,88,180405.